ministerie van verkeer en waterstaat

koninklijk nederlands meteorologisch instituut

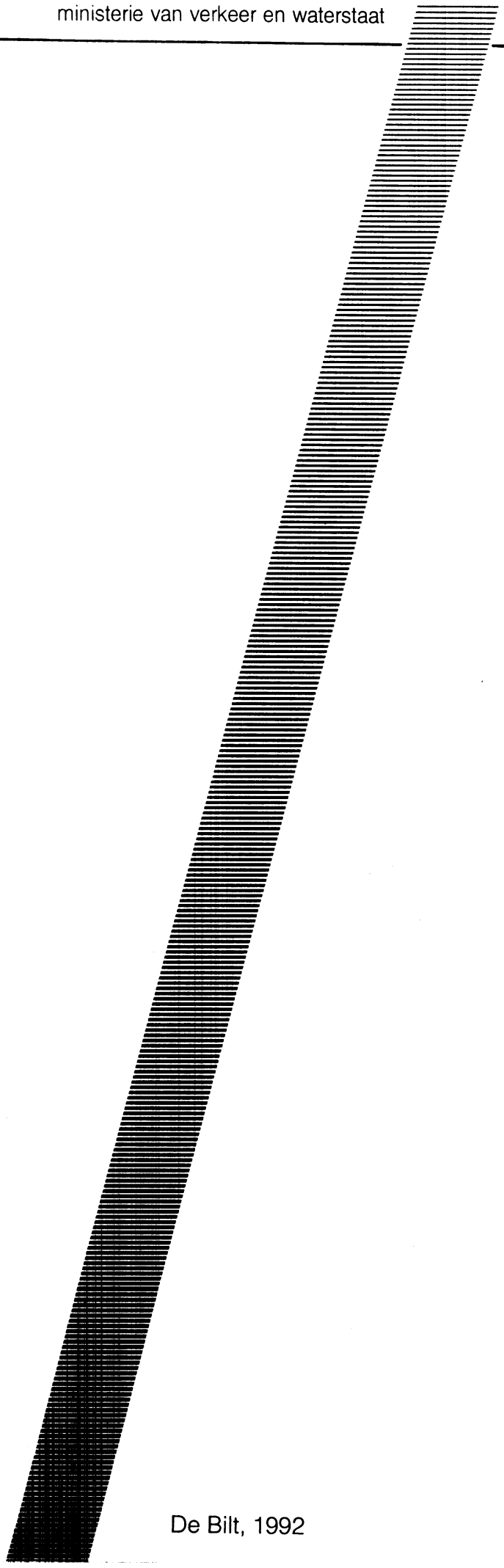

The Earth Radiation Budget Experiment: overview of data-processing and error sources

Arnout J. Feijt

Technical reports; TR-146
Technische rapporten; TR-146

De Bilt, 1992

de bilt 1992

publicationnummer: Technical reports=
technische rapporten; TR-146

p.o. box 201
3730 AE de bilt
wilhelminalaan 10
tel. (030) 206911
telex 47096
fax (030) 210407

U.D.C.: 551.501.721
551.506.2
551.508.25

ISSN: 0169-1708

ISBN: 90-369-2024-8

Abstract

The Earth Radiation Budget Experiment provides global information on the radiation properties of the Earth's atmosphere and surface. This report describes the data-processing scheme, which is used to convert raw radiometer counts into values for radiant exitance at the top of the atmosphere. Error sources are evaluated. When possible, the magnitude of the errors is estimated. This is proven difficult, because the errors depend on surface characteristics, atmospheric conditions, latitude, solar zenith angle and the viewing geometry. Most scanner measurements have been processed and validated. When using monthly mean scanner values one should be aware that specific regions may show considerable biased values of the radiant exitance. The standard deviation in the regional monthly mean values is of the order of 5 W/m^2. Instantaneous scanner values should be used with caution, because errors in the radiant exitance values for shortwave radiation in the order of 45 W/m^2 are no exception. The error is highly dependent on viewing geometry, atmospheric conditions and latitude. Nonscanner data are not fully validated yet. Probably the errors will exceed those of the scanner.

Contents

1. Introduction

The Earth Radiation Budget (ERB) consists of three parts: the incident solar radiation and the outgoing longwave and shortwave radiation. The net radiation budget varies widely with location and time. Temporal variations in the budget are present on an annual, but also on a diurnal scale.

The Earth Radiation Budget Experiment (ERBE) is designed to measure the Earth radiation budget on a global scale (Barkstrom and Smith, 1986). The objectives of ERBE are:
(1) to determine for a minimum of one year, the monthly average radiation budget on regional, zonal and global scales.
(2) to determine the equator to pole gradient of the radiation budget
(3) to determine the average diurnal variation of the radiation budget on a regional and monthly scale.
A region is a 2.5x2.5 deg^2 area. A zone is a 10x10 deg^2 area.
ERBE consists of three satellites carrying an ERB instrument package. The instruments are scanning and nonscanning radiometers for the detection of solar incoming radiation, reflected (solar) shortwave radiation (0.2-5 μm) and emitted longwave radiation (5-50 μm). The parameters to be obtained are the incoming solar radiation and the outgoing shortwave and longwave radiation at the top of the atmosphere. The resulting ERBE archival products are listed in Table 1.

S-1 Raw radiometric counts,	daily
S-5 Orbital ground track plots on paper	daily
S-2 Solar irradiance from bi-weekly calibrations	monthly
S-8 Instantaneous scanner and nonscanner measurements inverted to top of the atmosphere	monthly
S-9 Regionally averaged scanner data	monthly
S-10 Regionally averaged nonscanner data	monthly
S-4 Regional, zonal and global averages of longwave shortwave radiation and albedo	monthly
S-7 Instantaneous nonscanner measurements inverted to the top of the atmosphere	monthly

Table 1. ERBE archival products

Although it may seem simple to measure these quantities, the ERBE data-processing is complicated due to variations in surface and atmospheric properties affecting the emittance, reflectance and transfer of radiation. In the next sections a technical description of the ERBE data-processing scheme is given. Physical quantities are defined in Appendix A.

	required (W/m^2)	ERBE capacity (W/m^2)
1000 km zones	2-12 LW	5.2 LW
	2-12 SW	5.3 SW
1000 km regions	2-15 LW	9.4 LW
	2-15 SW	10.3 SW
250-500 km regions	2-14 LW	9.4 LW
	2-14 SW	10.3 SW
Global, net	1 (net)	1.3 (net)
Equator to pole gradient	4 (net)	2 (net)

Table 2. Accuracies of radiant exitance to be determined at top of the atmosphere (TOA). LW, longwave radiation; SW, shortwave radiation; net, incoming SW radiation minus outgoing SW and LW radiation; (source: Barkstrom and Smith, 1986)

The results from the ERB Experiment can be used to improve the understanding of heat transfer and thereby improve weather forecasting. Another application of the ERBE data is verifying General Circulation Models (GCM). The ERBE dataset will also be useful as an archive of the weather conditions during the time ERBE

is operational. In the years to come this dataset can be compared with future similar datasets. This can give valuable information on climate change. To increase the usefulness of the ERBE dataset a special data-processing branch is created for clear sky values. Because of these target applications the retrieved ERB values will need an unprecedented accuracy. The required accuracies and the designed ERBE capabilities are listed in Table 2.

2. Instruments

2.1 The three satellite system

Estimates of the diurnal variations in the local ERB can be seriously wrong if extrapolated from one or two measurements per day as is done by one satellite. This is clearly illustrated in Fig.1. The objective concerning the measurement of the diurnal cycle is met by defining a three-satellite system: two sun-synchronous polar satellites plus the special purpose Earth Radiation Budget Satellite (ERBS). A comparison between errors related to one, two and three satellite systems is given in paragraph 7.1.5. The three satellites involved are listed in Table 3.

name		ERBS	NOAA-9	NOAA-10
flight name		ERBS	NOAA-F	NOAA-G
altitude		600 km	872 km	833 km
footprint		31x47 km^2	44x65 km^2	44x65 km^2
inclination		57 deg	98 deg	98 deg
equator crossing time		varying	07.30 LT	19.30 LT
precessing period		37 days	-	-
launch date		05-10-1984	12-12-1984	17-09-1986
scanner data-collection	start	05-11-1984	05-01-1985	12-11-1986
	end	02-1990	01-1987	05-1989

Table 3. Satellites involved in ERBE.

2.2 Scanner

The scanner instrument is described in detail by Kopia (1986). It consists of three narrow field of view (NFOV) radiometers. The spectral response functions of the three channels are shown in Fig.2. The instrument channels are designed to have the following spectral range:

SW : 0.2 - 5 μm
LW : 5 - 50 μm
Total : 0.2 - > 50 μm

In an article by Barkstrom et al. (1989) the following values are given:

SW : 0.2 - 4.5 μm
LW : 6 - 36 μm
Total : 0.15 - 200 μm

Apparently, the operational range differs from the designed range.

The scanner is shown in Fig.3. It consists of detectors mounted on a scan head. The scan head can rotate so that the elevation angle varies from 14 to 240 deg. Nadir is at 90 deg and internal calibration at 190 (see Fig.4). The scan head can also rotate in the azimuth direction. The scan speed is 66.7 deg per second. One scan cycle, which includes calibration and resetting, takes 4 seconds. While scanning data is taken at a rate of 30 pixels per second per channel. When calibration and resetting is taken into account, the average data-collection rate is 14 pixels per second per channel. This means a total of 1.3 million pixels per day per

channel. The viewing aperture is a 3x4.5 deg^2 hexagon. This means a footprint of 31x47 km^2 at nadir for ERBS at 600 km altitude, and a footprint of 44x65 km^2 for the NOAA satellites at 850 km altitude. The sun-synchroneous satellites move at a speed of 360 deg per 102 minutes which is 0.06 deg/s. During one measurement the sub-satellite point moves 0.2 km. The digital accuracy is 12-bits.

2.3 Nonscanner

The nonscanner instrument, shown in Fig.5, is described in detail by Luther et al. (1986). It consists of a medium field of view (MFOV) and a wide field of view (WFOV) radiometer to measure the Earth's reflected solar and emitted radiation and a Solar Monitor Assembly (SMA) to measure the incident solar flux. The WFOV is designed to view the Earth from limb-to-limb. For a satellite at 800 km altitude the nadir-to-limb angle is 63 deg and the corresponding Earth central angle is 27.5 deg (see Fig.7). So the total field of view (from limb-to-limb) is 126 deg. The MFOV radiometer is designed to view a 10 deg Earth central angle. Since the ERBS satellite has a lower altitude, the viewing aperture is larger than that of the NOAA satellites and the corresponding Earth central angle is smaller. The nonscanner instrument has a SW, LW and Total channel, like the scanner. The nonscanner radiometers take a sample each 0.8 s to create a 13-bits digital output. In that time the satellite moves 0.05 deg and the sub-satellite point moves 5 km.

3. Scanner data-processing

Scanner data is converted to radiant exitance at the top of the atmosphere. The steps in the simplified data-processing scheme for scanner data are:

(1) conversion from counts to radiance
(2) conversion from radiance to radiant exitance
(3) spatial and temporal averaging

The main problems in retrieving radiant exitance values at the top of the atmosphere are:

(1) The detectors used are broadband radiometers, with a specific response function (see Fig.2). The incoming signal must be corrected for this spectral response function of the detector. But to do this one should know the spectral signature of the incoming radiation, which we do not know.
(2) It is not possible to measure directly the radiant exitance at the top of the atmosphere, because then one would need a device to measure similtaneously the radiances from each location at all viewing angles. The angular distribution of (reflected SW) radiance can vary widely. The inversion algorithm calculates radiant exitance values from single measured radiances.
(3) The albedo is dependent on local surface features and the solar zenith angle.

The spectral signature, angular distribution of radiance and albedo of each individual scene is different. They depend on surface features, cloud distribution and viewing geometry. Therefore, ERBE data-processing approach defines 12 types of observed scenes to diminish these problems. There are four types of surface: ocean, land, snow/ice and desert, and four types of cloud cover: clear, partly cloudy, mostly cloudy and overcast. Definition of cloud fraction: 0-5% clear, 5-50% partly cloudy, 50-95% mostly cloudy, 95-100% overcast. Definition of coastal: more than 33% water and more than 33% land. The scene types are listed in Table 4.

1 ocean	clear
2 land	clear
3 snow/ice	clear
4 desert	clear
5 coastal	clear
6 ocean	partly cloudy
7 ocean	mostly cloudy
8 land	partly cloudy
9 land	mostly cloudy
10 coastal	partly cloudy
11 coastal	mostly cloudy
12 overcast	

Table 4: The 12 ERBE scene types

Characteristics of the 12 scene types are used as reference values in the ERBE data-processing. In the next section a description is given of these reference values, their features and their origin.

3.1 ERBE reference database

Measurements from the Nimbus-7 instruments provide the primary source of information for the scene type characteristics. The Nimbus-7 instruments contain among others an ERB scanning radiometer, a Temperature and Humidity Infrared Radiometer (THIR) and a Total Ozone Mapping Spectrometer (TOMS). The ERB instrument is similar to the ERBE instrument and is described in detail by Jacobowitz et al. (1984). Measurements from Nimbus-7 were processed using methods described by Taylor and Stowe (1984). Also data from the GOES geo-stationary satellite were used. The main drawback using the GOES data is that each surface spot is always seen at the same viewing angle.

Each Nimbus-7 measurement is assigned to a scene type using geographical information combined with a cloud-detection algorithm. From each measurement the surface features are derived using geographical information. The cloud fraction is derived from measurements of the THIR and TOMS detectors and a surface temperature analysis from 3-hourly, 3-D nephanalysis data (Stowe et al., 1988). The measurement is assigned to a scene type, and is used to obtain reference values for the following scene type characteristics:

(1) anisotropic function for shortwave radiation
(2) standard deviation of mean radiance for shortwave radiation
(3) shortwave-longwave correlation coefficient
(4) albedo
(5) anisotropic function for longwave radiation
(6) mean radiant exitance for longwave radiation
(7) standard deviation of mean radiance for longwave radiation
(8) spectral correction matrices (explained in the next section).

The first four characteristics together are called the angular dependence model (ADM) for shortwave radiation. Values are obtained per scene type, solar zenith angle and azimuth angle. The next three characteristics are called the ADM for longwave radiation. Values are obtained per scene type, latitude and time of year.

To describe the angular variation of radiance, the angular coordinates are divided into ranges called "bins". There are 10 solar zenith angle bins, 7 viewing zenith angle bins and 8 azimuth angle bins. Latitudes are divided into 10 bins. The time of year is divided into 4 seasons; winter is defined as Dec, Jan, Feb. Obviously, a huge amount of data is needed to fill the bins. For example, per scene type the shortwave radiation model has 10x7x8 = 560 bins. The creators of the ADMs had to use inter- and extrapolations, symmetry mappings etc. to get trustworthy values for each bin. Henceforth, the reference database will be referred to as the N7-database.

More information about the databases can be found in :

- SW ADM and albedo : Suttles et al. (1988)
- LW ADM : Suttles et al. (1989)
- Spectral correction matrix : Avis et al. (1984)

The data-processing scheme for scanner data is shown in Fig.8. In the next sections the processing steps will be described.

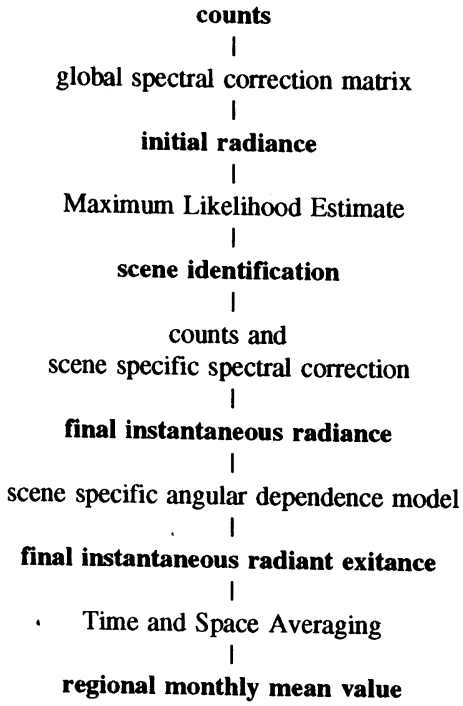

Fig. 8: Data-processing steps for scanner measurements. Bold, intermediate products; normal, used tools and reference values.

3.2 Spectral conversion

As described above, the relation between counts and radiance depends on the spectral distribution of the incoming radiation, which depends on the scene. From the Nimbus-7 measurements values have been derived for matrices which convert counts for all three channels into SW and LW radiances. Each scene type has its own conversion matrix. The radiance is calculated from the counts using the equation:

$$\begin{pmatrix} Radiance_{SW} \\ Radiance_{LW} \end{pmatrix} = C_{SceneType} \begin{pmatrix} counts_{SW} \\ counts_{LW} \\ counts_{Tot} \end{pmatrix} \qquad (1)$$

$C_{SceneType}$ is a conversion matrix (2x3) of regression coefficients for each scene type. There are 13 conversion matrices, one for each scene type and one neutral. The neutral matrix is used to obtain initial values for radiances, which are used to identify the scene type. The scene identification method is called the Maximum Likelihood Estimation (MLE) and is described in the next section.

4. Maximum Likelihood Estimation (MLE)

The MLE methodology (Wielicki and Green, 1989) is used to identify the scene type. If the scene type is known, the N7-database can be used to calculate the physical quantities of interest. In this section the MLE concept is described.

The first step is to identify the surface type from geographical information. Next the cloud fraction is to be identified. There are four categories: clear, partly cloudy, mostly cloudy and overcast. For each of these four cloud cover categories the probability that the measured radiance pair, SW and LW, is related to that category is calculated. The probabilities are calculated using reference values from the N7-database. The category with the highest probability is chosen to be the observed cloud fraction. The reference values corresponding to this scene type are used to calculate the final radiance and radiant exitance. A graphical representation of the method is shown in Fig.9.

5. Nonscanner data-processing

The MFOV and WFOV measurements are processed similarly. Two techniques are used to process the nonscanner data: the Shape Factor technique and the Numerical Filter (NF) technique. The Shape Factor technique is easy to apply and gives an estimate for the radiant exitance for the entire field of view. The NF method is complicated, but gives results at a higher spatial resolution, 5x5 deg^2.

5.1 Shape Factor method

5.1.1 Shape Factor method for longwave radiation

The Shape Factor method for longwave radiation assumes the radiant exitance to be constant over the field of view. Then one can derive:

$$RadiantExitance = \frac{counts}{SF} \tag{2}$$

SF is the anisotropic factor averaged over the field of view and weighted by the angle of incidence. For each 2.5x2.5 deg^2 region the scene type is obtained from the scanner data-processing. The contribution of each specific region depends on the viewing zenith angle for that region and the position of the region in the field of view.

5.1.2 Shape Factor method for shortwave radiation

When analyzing shortwave radiation the albedo, a, and the irradiance, E, are taken to be constant over the field of view. Similar to the equation above one can derive:

$$RadiantExitance = \frac{counts}{(a*E*SF)} \tag{3}$$

The contribution of each region in the field of view to the total signal depends on the regional solar zenith angle, the regional anisotropic function and the angular position of the region in the field of view. These characteristics are integrated over the total field of view to obtain *SF*. The regional averaged albedo and anisotropic factor are derived from scanner data.

In absence of scanner data, scene identification defaults to preprogrammed scene information based on climatology.

5.2 Numerical Filter method

In this section the Numerical Filter method is described at a conceptual level. A full description is given by Green (1983). The Numerical Filter method uses the fact that successive measurements overlap to increase the spatial resolution. From limb-to-limb the WFOV measures the radiance coming from a 55 deg Earth central angle. Each measurement is taken 0.8 s or 0.05 deg apart. This means that each strip of 0.05 deg width contributes to approximately 1000 measurements. In Fig.10 the spatial geometry is shown. In the Numerical Filter method the field of view is divided into strips. These strips do not directly correspond to the measurement strips described above. If one defines the radiant exitance, M, to be constant for an entire strip, one can assign a weight factor, y, to the contribution of each strip to a specific measurement:

$$measurement = \sum_{i=0}^{N} y(i)M(i) \tag{4}$$

where i indicates the contributing strip. N denotes the number of strips per measurement. Reversely, there are J measurements which contribute to one strip, because the measurements overlap:

$$M(i) = \sum_{j=0}^{J} w(j)measurement(j) \tag{5}$$

there j indicates the contributing measurement, and $w(j)$ is a weight factor. N and J are chosen parameters; N corresponds to the spatial resolution and J corresponds to the accuracy. On the other hand, the accuracy is inversely related to N. The process parameters N and J are optimized to obtain a 5x5 deg^2 resolution and a minimum error.

The scanner data and the N7-database are used to get values for the spectral correction matrix, the anisotropic function, etc. In the absence of scanner data, scene identification defaults to preprogrammed scene information based on climatology.

6. Time and Space Averaging

The Time and Space Averaging (TSA) is developed to obtain regional, zonal and global values for mean monthly radiant exitance and the monthly diurnal variation in radiant exitance. The input to the TSA are the instantaneous SW and LW radiant exitance and the solar irradiance. The TSA algorithms are described in detail by Brooks et al. (1986).

6.1 Scanner

Each retrieved instantaneous radiant exitance value is assigned to an ERBE region. There are 10,368 regions, which are all 2.5x2.5 deg^2. All measurements from one month are stored in a monthly regional data matrix. The matrix has entries for each day of the month and for each hour of the day. So for January the matrix consists of 31x24=744 entries. There can be many measurements in an one-hour box. All scene types are assumed to contribute linearly to the regional radiant exitance. The LW radiation changes slow with time, so that all LW values in a one-hour box are averaged with the same weight. The SW measurements, however, have to be corrected for the change in insolation and albedo with time. The time center of each hour box, the half hour, is taken to be the reference time for the box. For each measurement the apparent reference time value is calculated. The albedo depends on the scene type, so the N7-database is used here.

There are 10,368x24=248,832 hour boxes to be filled. Not surprisingly there are many empty hour boxes. The TSA uses different interpolation methods for SW and LW radiation to fill all the boxes. The LW boxes are filled using linear interpolation from available measurements. However, for some regions, e.g. desert, a

half-sinus model is used to account for diurnal variations. If a SW hour box is empty the closest left and right measurements are combined. Both measurement values are extrapolated to the target hour box. As described above this involves also insolation and albedo extrapolation. Then the two extrapolated values are added weighted by their time-distance to the target hour box. In order for this interpolation method to be valid the following assumptions are made: the scene type does not change between the hour boxes, the measured scene type is correct and the variation in time of the albedo is known.
There are two ways to calculate the monthly mean radiant exitance: using all interpolated values, or only using those days which have measured values. In the last case the days selected should be representative of the month. If the two monthly means differ too much there are sampling problems.

6.2 Nonscanner

The nonscanner input to the TSA are the radiant exitance derived from the Shape Factor method and the radiant exitance derived from the Numeric Filter method. The Shape Factor values correspond to a 10x10 deg^2 area centered around the sub-satellite point. The Numerical Filter values correspond to a 5x5 deg^2 area, also beneath the satellite.
The conversion from inflight coordinates to the ERBE 5x5 and 10x10 grids is straightforward. The measurement is entered into the regional data matrix belonging to the region the sub-satellite point was in at the time of the measurement. As a result only data for those regions which are part of the satellites ground-track are obtained. This effect is accounted for by zonal averaging at the end of the TSA processing.
The TSA process for nonscanner data uses scanner scene type information for inter- and extrapolation purposes. In the absence of scanner data, scene identification defaults to preprogrammed scene information based on climatology.

7. Error analysis

In this section the various error sources are described. When possible, the magnitude of errors is estimated. The complexity of the error analysis mirrors the complexity of the data-processing as described above. There are many error sources, which are often interrelated. Most clearly visible are the measurement errors in the radiometers. The least visible are the errors which originate from the use of the N7-database.
In section 7.1 the errors in the scanner data-processing are described. The error sources for the scanner instrument value of radiant exitances are: instrument, sampling, MLE-scene identification, spectral correction, longwave angular dependence model, shortwave angular dependence model and time/space sampling. Most error sources in the scanner data-processing scheme indirectly affect the nonscanner results. At the end some specific errors in the nonscanner data-processing scheme are evaluated.

7.1 Scanner errors

7.1.1 Scanner instrument
The scanner instrument has in-flight calibration facilities. Instrument errors for the scanner radiometers are listed in Table 5 (Kopia, 1986).

	3 sigma ($W/m^2/sr$)	sys. error bound ($W/m^2/sr$)
SW	0.3	0.75
LW	0.45	0.75
Total	0.3	0.5

Table 5. ERBE scanner standard deviation and a measure for the systematic error for the measured radiance. To obtain the error of the related radiant exitance the tabulated values should be multiplied by π (which holds for a Lambertian surface), which yields approximately 1 W/m^2 for the 3 sigma error.

7.1.2 Sampling errors

7.1.2.1 Field of view nonuniformity
Within the field of view of the scanner (footprint at nadir 44x64km^2) the scene may consist of a mixture of clouds, snow, land and lakes. In these cases the scene identification algorithm will not be very decisive.

7.1.2.2 Variable spatial coverage
As the scanner field of view moves from nadir to limb the footprint increases from 44x64km^2 to more than 250x250km^2. At nadir a region is covered by approximately 20 scanner pixels. At the limb two pixels cover the same area. Moreover, these two pixels limb may overlap.

7.1.2.3 Viewing zenith angle and broken clouds
A warm surface with a partial cloud cover of high, cold clouds will seem colder to the LW radiometer if the viewing zenith angle increases. The scanner will look more and more at the side of the cloud which increases the apparent cloud cover. Cloud sides can also change the SW reflected solar radiation markedly.

7.1.3 Maximum Likelihood Estimate method
The ERBE scene type identification through the MLE method has proven to be not reliable. Diekmann and Smith (1989) investigated the misidentification problem by intercomparing the results from the MLE method with results using Advanced Very High Resolution Radiometer (AVHRR) data. The intercomparison shows that there is a tendency for underestimating cloudiness over ocean at high cloud amounts, for example partly cloudy instead of mostly cloudy. On the other hand clear ocean scenes are often misclassified (compared to AVHRR scenes) as partly cloudy.

7.1.4 N7-database
In many places in the ERBE data-processing sequence the N7-database is used. Although the N7-database is of crucial importance, its reliability has hardly been evaluated. In this section an attempt is made.

7.1.4.1 LW anisotropic function
In Fig.11 a number of longwave anisotropic functions is shown. From the Nimbus-7 measurements a huge amount of anisotropic functions has been derived for different latitudes and seasons. All these anisotropic functions look alike. So the dependence of the radiance on the viewing zenith angle for longwave radiation hardly varies with latitude or season. Therefor errors in scene type identification will hardly have an effect on the longwave angular distribution of radiances.
In Fig.12 the dispersion of longwave radiances for land and ocean scenes is shown. The dispersion is defined as standard deviation over mean value. In the figure all viewing angles and seasons are averaged. The dispersion varies from 3% for tropical clear sky to up to 24% for tropical overcast. The dispersion is a measure for the merits of the classification in 12 scene types. A large dispersion means that there is a large variety of values within the scene type. From the figure it is clear that "overcast" is a doubtful classification. This is not really surprising, because overcast clouds can as well be high cirrus as low stratus. These cloud types emit longwave radiation differently. In general the dispersion in longwave radiation increases with increasing cloud cover.

7.1.4.2 SW anisotropic function
In Fig.13 some examples of SW anisotropic functions are shown. The anisotropic factor varies widely with viewing angle. Clearly the anisotropic functions vary markedly with cloud cover. This implies that misinterpretation of the amount of cloud cover will lead to significant errors in the obtained radiant exitance values.
In Fig.14 the dispersion of shortwave models averaged over all viewing angles and azimuths is shown. The dispersion ranges from 18 to 40%. The highest values correspond to partly and mostly cloudy scenes. It is well known that measurements of broken cloud fields are hard to interpret. Theoretical studies by Davies (1984) and an analysis of satellite measurements by Coakley and Davies(1986) have shown that the 3-dimensional structure of broken clouds strongly influences the reflected radiances, e.g. by reflections from the sides of the clouds. In contrast with the longwave case overcast situations show relatively little dispersion. In contrast to the emission of longwave radiation, reflection of shortwave radiation is hardly

dependent on the cloud height.

A large dispersion of anisotropic factors has a considerable impact on the interpretation of separate measurements. The anisotropic factor used in the data-processing are bin averages. Because the dispersion within a bin is large, the mean anisotropic factor will differ considerably from the precise anisotropic factor for the specific measurement. This results in an unreliable value for the radiant exitance derived from individual radiance measurements. The error originating from the scatter within one anisotropic factor-bin reduces if the number of measurements increases. This assumption, which is widely accepted, has a pitfall. The assumption only holds if the measurement conditions and the conditions during the creation of the N7-database are similar. One would expect that a region which has exceptional surface characteristics or cloud type will show a biased calculated radiant exitance.
Fig.13 and 14 show that the dispersion of anisotropic factors for clear sky situations are relatively small. Therefor the standard deviation in clear sky values will be smaller.

7.1.4.3 Albedo
In Fig.15 the N7-database values for albedo are shown. The albedo is highly dependent on cloud cover. This means that errors in scene type identification have a large impact on the interpretation of the measurement. I have not found any publication which could give insight into the validity of the albedo values.

7.1.4.4 Errors due to the use of ADMs as derived from a simulation
Stowe et al. (1991) studied the contribution of the errors in the ADMs to the errors in the resulting SW radiant exitance. They concluded that if systematic ADM errors are less than 30%, as suggested in various articles, the ERBE standard deviation of the instantaneous radiant exitance due to the use of ADMs derived from the N7-database is about 13 W/m^2. The errors in the LW radiant exitance values are about 25% of the shortwave errors. The contribution of the errors in the ADMs to individual measurement values depends on the viewing geometry and the scene type. Some of Stowe et al.'s figures show areas with radiant exitance errors of up to 45 W/m^2. Scene type misidentification gives rise to errors ranging from 15 to 45 W/m^2.

7.1.5 Time sampling
The TSA uses inter- and extrapolation of measurements in order to fill all hour boxes for the regional monthly data matrix. The errors resulting from time sampling depend on the interval between measurements and therefor on the number of satellites involved (Brooks et al., 1986). Brooks and Minnis (1984) simulated data retrieval using the TSA to obtain insight in the relation between sample rate (number of satellites involved) and the bias and rms errors. In Table 6 some results are listed.

satellites involved	bias range (W/m^2)	stand. deviation (W/m^2)
NOAA-9 + ERBS	+2 / +3	6 / 11
NOAA-10 + ERBS	-3 / -1	3 / 7
NOAA-9 + 10 + ERBS	+0.7 / +1	2 / 3

Table 6. Time sampling errors of the net radiation derived by Brooks and Minnis (1984) for various satellite configurations.

7.1.6 Total error estimates on the basis of reference measurements
From the first results, obtained in April 1985, the ERBE science team has derived estimates for the standard deviations in the measurements (Barkstrom et al., 1989). These are:
For instantaneous radiances:
LW 1%
SW 2-3%
For instantaneous radiant exitance:
LW 5 W/m^2
SW 15 W/m^2

For monthly averaged scanner derived radiant exitance:
LW 5 W/m^2
SW 5 W/m^2
For global annual average:
NET 5 W/m^2

Harrison et al. (1990) have given an overview of the error estimates reported so far. From this text we give a summary below.
Largest contributions to the errors originate from misclassification of particular scene types and sampling deficiencies. Misclassification may result in biases in the radiant exitance for a specific scene type. Sampling errors occur when not all variations in meteorology and optical properties are accounted for. ERBE identifies snow-covered scenes as either clear or overcast. The scene identification algorithm over snow is considered highly unreliable. Large errors due to misclassification of clear-sky over land situations are found. Evidence from a study by Hartmann and Doelling suggests that the nighttime, clear-sky longwave flux over oceans may be overestimated by about 6-7 W/m^2.

Schmetz et al. (1990) suggest that all ERBE longwave clear sky fluxes are likely to possess a bias of 3-5 W/m^2 due to the influence of the upper tropospheric humidity on the radiation field.

7.2 Some specific nonscanner errors

7.2.1 Nonscanner instrument
The nonscanner instrument also has in-flight calibration facilities. Instrument errors from the nonscanner radiometers are listed in Table 7 (Luther et al., 1986).

	3 sigma (W/m^2)	systematic error (W/m^2)
MFOV,total	2.0	3.3(2.4)
MFOV,SW	2.3	4.5(3.0)
WFOV,total	2.6	4.0(1.7)
WFOV,SW	2.5	6.0(3.8)
SMA	4.2(2.8)	7.0(1.4)

Table 7. ERBE nonscanner standard deviation and systematic error of the measured radiant exitance.

7.2.2 Shape Factor
The accuracies of the Shape Factor method flux estimates are investigated by Green and Smith (1991). They simulated the inversion technique with ERBE scanner data. The standard deviation of the MFOV errors was 12 W/m^2, and for WFOV errors 21 W/m^2. The magnitude of the biases for both cases were less than 1 W/m^2.

7.2.3 Numerical Filter
Using the NF method the spatial resolution can be enhanced, but at the price of an additional error source. The error depends on the target spatial resolution and the number of measurements involved in calculating the radiant exitance for one area. The target area is chosen to be 5x5 deg^2 Earth central angle. The number of measurements involved is optimized in order to reduce the error. To obtain the optimum Green (1983) performed a case study. The Nimbus-6 data for one, 102 minute, orbit were used to generate a truth set. Then the truth was converted to synthetic measurement values. Assuming error-free angular dependence models and error-free measurements Green suggests that the standard deviation of the radiant exitance averaged over a 5x5 deg^2 region is about 3 W/m^2. Random measurement errors where introduced with a 1 W/m^2 standard deviation error. Including these measurement errors Green suggests that the standard deviation of the radiant exitance averaged over a 5x5 deg^2 region is about 4 W/m^2, assuming perfect ADMs.

8. Conclusions about errors

The main error source in the retrieval is the use of the N7-database. The standard deviation of the anisotropic factor is about 30%. As a result, the calculated values of the instantaneous radiant exitance using the appropriate scene type anisotropic factor can easily miss the real value by 45 W/m^2.
Additionally, the scene identification can easily be wrong by one class. This holds especially at night, when only LW radiation can be used as input to the MLE. This can introduce additional errors in the instantaneous radiant exitance measurements of about 40 W/m^2.
The balancing feature is the huge amount of measurements which are performed. If one calculates monthly averages, the bias will vanish if the evaluated dataset contains the same variations as the N7-database. If one observes a region with exceptional surface characteristics or an exceptional cloud type, one can expect biased radiant exitance values.
From Fig.16 one can conclude that the three satellite scanning system lasted less than three months due to an unfortunate coincidence. The NOAA-9 scanner barely outlived its design lifetime of two years and the launch of NOAA-G was delayed for half a year. From Table 6 one can conclude that the remaining system, NOAA-10 plus ERBS, has a standard deviation of the time sampling error twice that of the three satellite system.
The failure of the NOAA-9 scanner has another drawback. The data-processing of the nonscanner instruments on NOAA-9 uses the scanner results to obtain information about the state of the atmosphere in the field of view. Because the scanner failed, the data-processing fell back on preprogrammed climatology values which are less reliable.

9. Discussion

9.1 Usefulness of ERBE data

Fig.16 shows the current state of data-processing. Most scanner measurements are processed and validated. When using monthly mean scanner values one should be aware that specific regions show considerable biased values. The standard deviations in the regional monthly mean values are of the order of 5 W/m^2. Instantaneous scanner values should be used with caution, because the accuracy is highly dependent on the viewing geometry and scene type. The accuracy can be increased considerably by choosing viewing geometries with corresponding anisotropic factors near unity. Errors due to scene misidentification and ADMs internal errors will then be relatively small.
The nonscanner measurements are still to be reviewed, so they are not available yet. Probably the errors in the nonscanner measurements will exceed those of the scanner measurements due to the more complicated data-processing scheme and the dependence on scanner data. When the scanner instrument has stopped operation, another error is introduced. Then the nonscanner data-processing scheme uses climatology data instead of the scanner data.

9.2 Examples of use of ERBE data

ERBE data has been used for many different purposes (Hartmann et al., 1986; Ramanathan, 1987). From a picture of the monthly mean regional radiative exitance one can get an idea of the spatial distribution of outgoing longwave radiation. Subtraction of the outgoing shortwave radiation from the insolation yields the radiation energy absorbed at each latitude and region. Combining the data of outgoing longwave radiation and absorbed solar energy yields values for the energy transport by atmospheric and oceanic currents. This information gives insight into the climate system. The ERBE data are also used to test GCMs (Smith, 1984). The calculated values of the outgoing longwave radiation should match the ERBE values. Also models for the calculation of atmospheric radiative flux profiles can be validated using ERBE data (Rossow et al., 1990). Recently ERBE data was used to calculate the influence of clouds on the Earth radiation budget (Ramanathan et al., 1989; Harrison et al., 1990). They calculated the cloud-radiative forcing on a global scale. Combination with cloud data from the International Satellite Cloud Climatology Project (ISCCP) can give information about the relation between cloud type and radiation.

9.3 Can ERBE data be upgraded

The basis of the ERBE data-processing scheme is the N7-database. The largest errors are due to the large dispersion in anisotropic functions and scene misidentification. To reduce the errors a new reference dataset should be developed. To this end a new set of scenes should be defined and characterized using the Nimbus-7 measurements. However, it seems hardly possible to define scene types with considerably lower dispersion. To reduce the chance of misidentification the Maximum Likelihood Estimate method should be improved. One could argue that there are more sophisticated ways to retrieve cloud amounts than the MLE method, which should reduce the chance of scene misidentification. The MLE method, however, is not created to retrieve values for cloud amount. Rather, it is a method to link real-time measurements to reference values, namely the N7-database. The MLE only calculates the probability that a measurement pair relates to a scene type from which many characteristics are known. Introducing another cloud amount retrieval method will not improve the link between measurement values and reference values and so will not solve the misidentification problem.

9.4 How to obtain ERBE data

A more detailed description of the ERBE data products is given by Barkstrom et al. (1989). ERBE data are available through the National Space Science Data Center (NSSDC). Outside the United States the address is World Data Center A, Rocket and Satellites, Code 630.2, Goddard Space Flight Center, Greenbelt, MD 20771, USA. Inside the United States the address is NSSDC, Code 633.4, Goddard Space Flight Center, Greenbelt, MD 20771.

Acknowledgements: I thank Dr. P. Stammes for revising this text and for his advice in the field of radiative transfer theory. This work is supported by the Dutch National Research Program on Global Air Pollution and Climate Change (NOP) under number 8520587.

REFERENCES

Avis, L. M., R. N. Green, J. T. Suttles and S. K. Gupta: A robust pseudoinverse spectral filter applied to the Earth Radiation Budget Experiment (ERBE) scanning channels, NASA Tech. Memo. TM-85781, 33 pp., 1984.

Barkstrom, B. R. and G. L. Smith: The Earth Radiation Budget Experiment: Science and implementation, Rev. Geophys, 24, no. 2, 379-390, 1986.

Barkstrom. B. R., E. Harrison, G. Smith, R. Green, J. Kibler, R. Cess and the ERBE Science team: Earth Radiation Budget Experiment (ERBE) Archival and April 1985 Results, Bull. Am. Meteorol. Soc., 70, 1254-1262, 1989.

Brooks, D. R. and P. Minnis: Simulations of the Earth's monthly regional radiation balance derived from satellite measurements, J. Clim. Appl. Meteorol., 23, 392-403, 1984.

Brooks, D. R., E. F. Harrison, P. Minnis, J. T. Suttles and R. S. Kandel: Development of algorithms for understanding the temporal and spatial variability of the Earth radiation balance, Rev Geophys., 24, 422-438, 1986.

Coakley, J. A. and R. Davies: The effect of cloud sides on reflected solar radiation as deduced from satellite observations, J. Atmos. Sci., 43, no. 10, 1025-1035, 1986.

Davies, R.: Reflected solar radiances from broken cloud scenes and the interpretation of scanner measurements, J. Geophys. Res., 89, no. D1, 1259-1266, 1984.

Diekmann, F. J. and G. L. Smith: Investigation of scene identification algorithms for radiation budget measurements, J. Geophys. Res., 94, no. D3, 3395-3412, 1989.

Green, R. N.: Accuracy and resolution of Earth radiation budget estimates, J. Atmos. Sci., 40, 977-985, 1983.

Green, R. N. and G. L. Smith: Shortwave shape factor inversion of Earth radiation budget observations, J. Atmos. Sci., 48, no. 3, 390-402, 1991.

Harrison E. F., P. Minnis, B. R. Barkstrom, V. Ramanathan, R. D. Cess and G. G. Gibson: Seasonal variation of cloud radiative forcing derived from the Earth Radiation Budget Experiment, J. Geophys. Res, 95, no. D11, 18,687-18,703, 1990.

Hartmann, D. L., V. Ramanathan, A. Berroir and G. E. Hunt: Earth radiation budget data and climate research, Rev. Geophys, 24, no. 2, 429-468, 1986.

Hartmann, D. L., and D. Doelling: On the net radiative effectiveness of clouds, J. Geophys. Res. 96, no. D1, 869-891, 1991.

Jacobowitz, H., H. V. Soule, H. L. Kyle, F. B. House and the ERB Experiment Team: The Earth Radiation Budget (ERB) Experiment: An Overview, J. Geophys. Res., 89, no. D4, 5021-5038, 1984.

Kopia, L. P.: Earth Radiation Budget Experiment scanner instrument, Rev. Geophys, 24, no 2, 400-406, 1986.

Luther, M. R., J. E. Cooper and G. R. Taylor: The Earth Radiation Budget Experiment non-scanner instrument, Rev. Geophys, 24, no 2, 391-399, 1986.

Ramanathan, V.: The role of Earth radiation budget studies in climate and general circulation research, J. Geophys. Res., 92, no. D4, 4075-4095, 1987.

Ramanathan, V., R. D. Cess, E. F. Harrison, P. Minnis, B. R. Barkstrom, E. Ahmad, D. Hartmann: Cloud-radiative forcing and climate: Results from the Earth Radiation Budget Experiment, Science, 243, 57-63, 1989.

Rossow, W. B., Y. Zang and A. A. Lacis: Calculations of atmospheric radiative flux profiles, 7th Am. Met. Soc. Conf. Atmos. Radiat., Boston, Mass., 81-86, 1990.

Schmetz, J., M. Mhita and L. van de Berg: METEOSAT observations of longwave cloud radiative forcing for april 1985, J. of Clim., 3, no. 7, 1990.

Smith, L. A., Radiative forcing of the southwest summer monsoon, Ph. D. thesis, 520 pp., Colo. State Univ., Fort Colins, 1984.

Smith, G. L., R. N. Green, E. Raschke, L. M. Avis, J. T. Suttles, B. A. Wielicki and R. Davies: Inversion methods for satellite studies of the Earth's radiation budget: Development of algorithms for the ERBE mission, Rev. Geophys, 24, no. 2, 407-421, 1986.

Stowe, L. L., C. G. Wellemeyere, T. F. Eck, H. Y. M. Yeh and the Nimbus-7 cloud data processing team: Nimbus-7 global cloud climatology. Part I: Algorithms and validation. J. Clim., 1, no. 5, 445-470, 1988.

Stowe, L. L., P. Ardunay, R. Hucek, P. Abel, H. Jacobowitz: Evaluating the design of satellite scanning radiometers for Earth Radiation Budget measurements with system simulations; Part I: Instantaneous estimates. NOAA Techn. Rep. NESDIS 58, 1991.

Suttles, J. T., R. N. Green, P. Minnnis, G. L. Smith, W. F. Staylor, B. A. Wielicki, I. J. Walker, D. F. Walker, D. F. Young, V. R. Taylor and L. L. Stowe: Angular radiation models for the Earth-atmosphere system. Vol I: Shortwave radiation. NASA Ref. Publ. RP-1184, 147pp., 1988.

Suttles, J. T., G. L. Smith, B. A. Wielicki, I. J. Walker, V. R. Taylor and L. L. Stowe: Angular radiation models for the Earth-atmosphere system. Vol II: Longwave radiation. NASA Ref. Publ. RP-1184, Vol. II, 87pp., 1989.

Taylor, V. R. and L. L. Stowe: Reflectance characteristics of uniform Earth and cloud surfaces derived from Nimbus-7 ERB. J. Geophys. Res., 89, no. D4, 4987-4996, 1984.

Wielicki, B. A. and R. N. Green: Cloud identification for ERBE radiative flux retrieval. J. Appl. Meteorol., 28, 1133-1146, 1989.

Appendix A

Radiation definitions

First we define the geometric symbols (see also Fig.6 and 7):

A : area (m^2), is always perpendicular to the surface normal
t : time (s)
ω : solid angle (sr)
θ : viewing zenith angle (deg), angle between the zenith direction and the direction to the satellite, as seen from the target area.
θ_0 : solar zenith angle (deg), angle between the zenith direction and the direction to the sun, as seen from the target area.
α : Earth central angle (deg), angle between two directions which intersect in the earth center
ϕ : azimuth angle (deg), angle between the plane through the surface normal and the incident solar radiation and the plane through the surface normal and the direction of the exiting radiation.

Next we define the radiation quantities:

Q : energy (J)
M : radiant exitance (W/m^2) (definition: $dQ/(dAdt)$)
the radiant exitance is the total amount of outgoing radiation per area, dA, and per time interval, dt.
E : irradiance (W/m^2) (definition: $dQ/(dAdt)$)
irradiance is the total amount of incoming radiation per area, dA, and per time interval, dt.
L : radiance ($W/m^2/sr$) (definition: $dQ/(dAdtd\omega\cos\theta)$)
radiance is the radiation in one specific direction per area, dA, per time interval, dt and per cosine of the (viewing) angle, θ, relative to the normal of the area.
R : anisotropic factor
the anisotropic factor is the dimensionless fraction of the radiant exitance in a specific direction. Stated differently, the anisotropic factor is the contribution of the radiance in a specific direction to the total radiant exitance (see Eq. A2).
a : albedo (definition: $dM/(E)$)
albedo is the fraction of the incoming radiation which is reflected

The scanner measures the integral of the radiance, $L(\theta,\phi)$, over the field of view. From this measurement we want to calculate the radiant exitance. By definition:

$$M = \int_0^{2\pi} \int_0^{\pi/2} L(\theta,\phi)\cos\theta\sin\theta d\theta d\phi \qquad \textbf{(A1)}$$

To perform this integration one should know the complete angular distribution of the radiance. We need to know the contribution of the measured radiance to the radiant exitance. This is given by the anisotropic factor, R:

$$R(\theta,\phi) = \frac{\pi L(\theta,\phi)}{M} \qquad \textbf{(A2)}$$

The symbol R is used both for the anisotropic factor as for the anisotropic function, which defines the anisotropic factor for all possible values of θ and ϕ.

The Lambertian definition of a diffusely reflecting surface states that the reflected radiance is independent of the viewing angle. This means that R equals one for all values of θ and ϕ. For such a surface:

$$M = \pi L(\theta,\phi) \tag{A3}$$

The relations above are a very simple representation of reality. The anisotropic factor not only depends on the viewing zenith angle and azimuth, but also on solar zenith angle, wavelength and surface features.

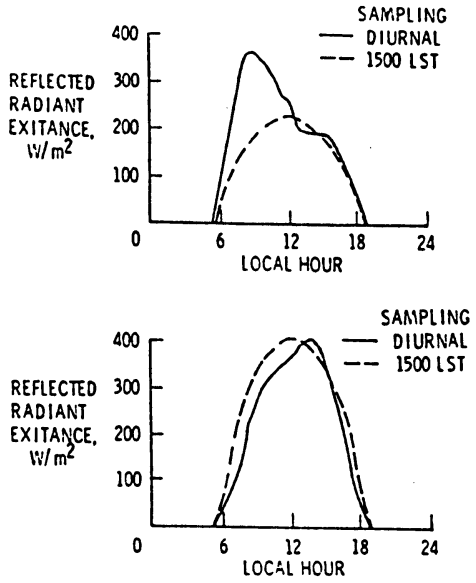

Fig. 1. Diurnal variation of reflected radiant exitance for two sites. Solid line, true value; dashed line, inferred value from a single satellite measurement at 1500 local time.

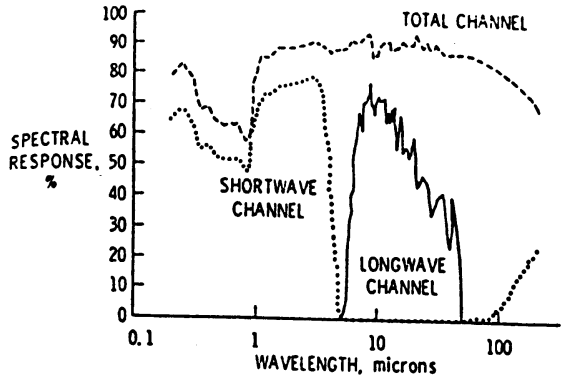

Fig. 2. Spectral responses of scanning radiometer channels.

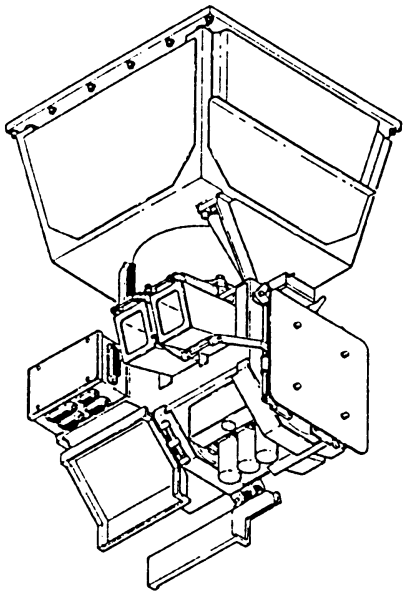

Fig. 3. ERBE scanner instrument

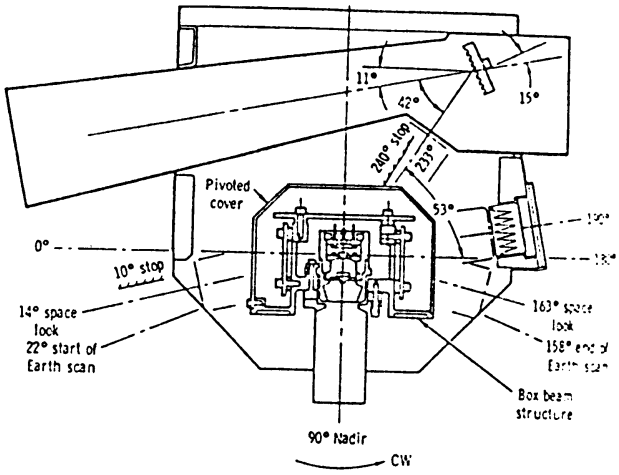

Fig. 4. Scanner elevation angles.

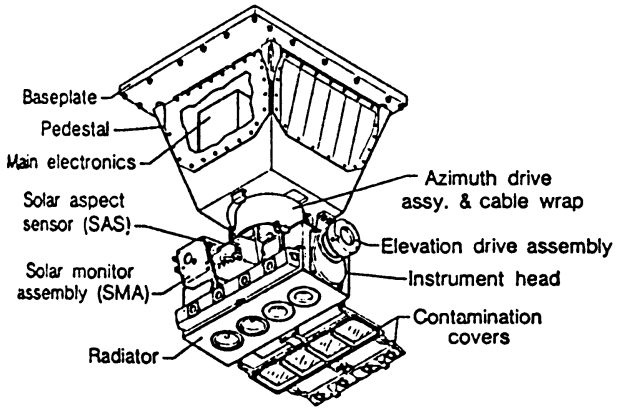

Fig. 5. ERBE nonscanner instrument.

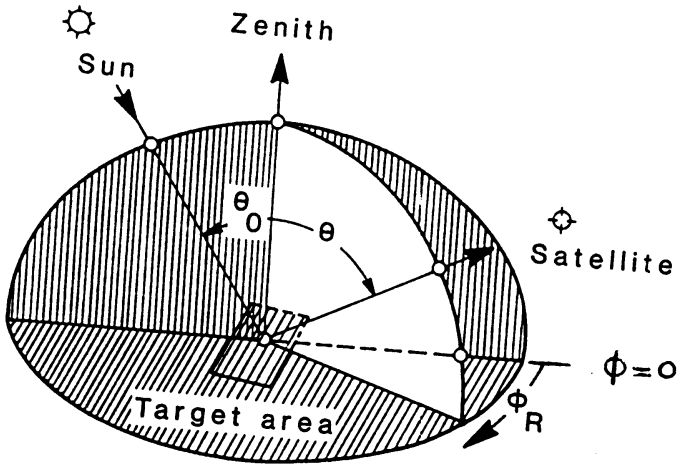

Fig. 6. Satellite, sun and target geometry.

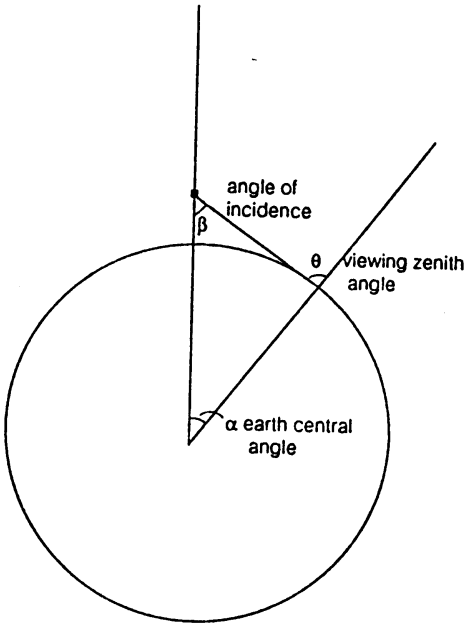

Fig. 7. Geometry of the zenith viewing angle (θ), the angle of incidence (β) and the earth central angle (α).

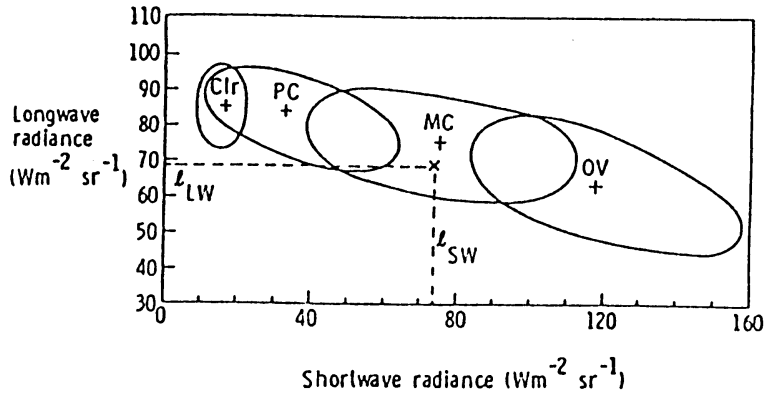

Fig. 9. Conceptual drawing of equiprobability ellipses for each of the four scene types: clear (clr), partly cloudy (pc), mostly cloudy (mc) and overcast (ov).

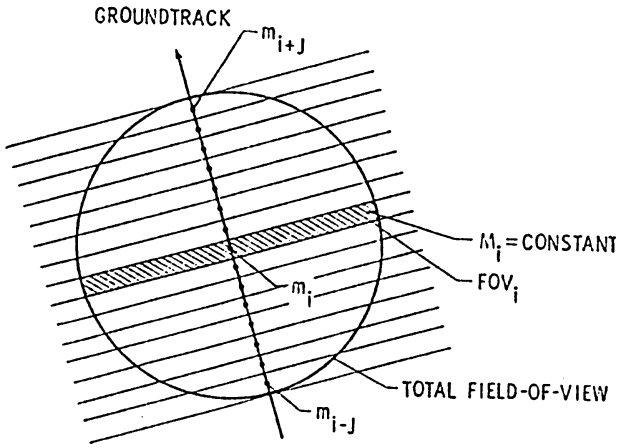

Fig. 10. Spatial geometry. The circle indicates the field of view. Each strip contributes to the measurement.

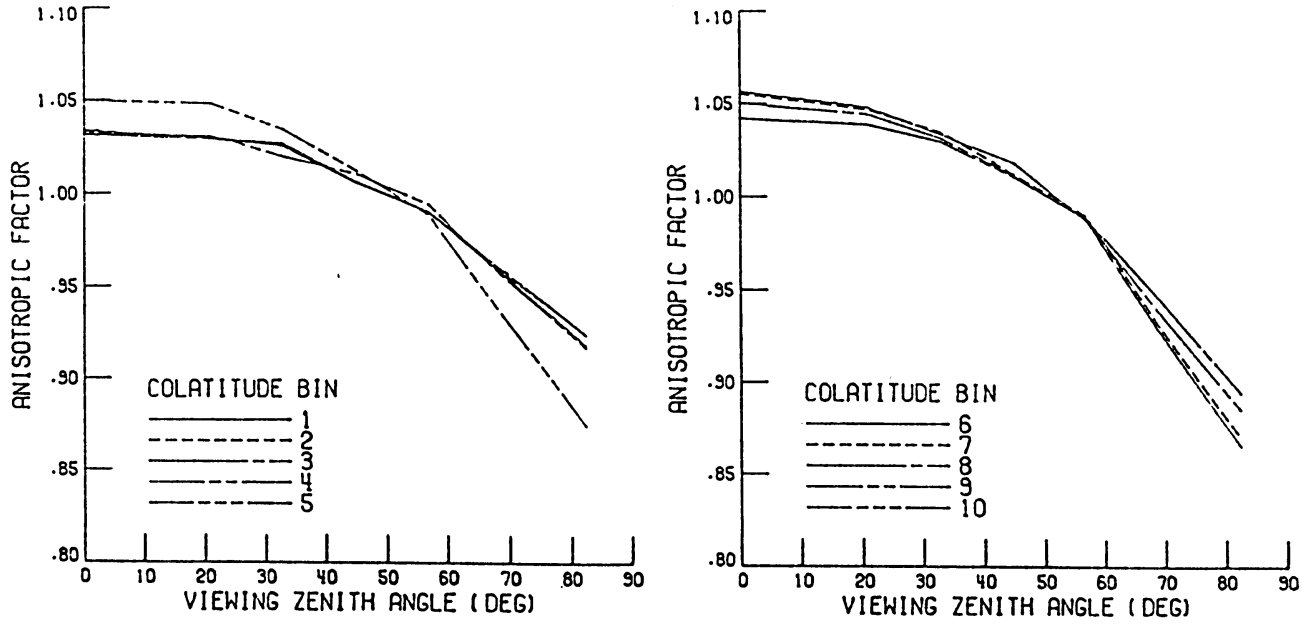

Fig. 11a. Longwave anisotropic factor, R, over land in winter, clear sky. Colatitude is (90 - latitude). Colatitude bins indicate latitude ranges: bin 1 is related to the north pole, bin 8 is related to the south pole.

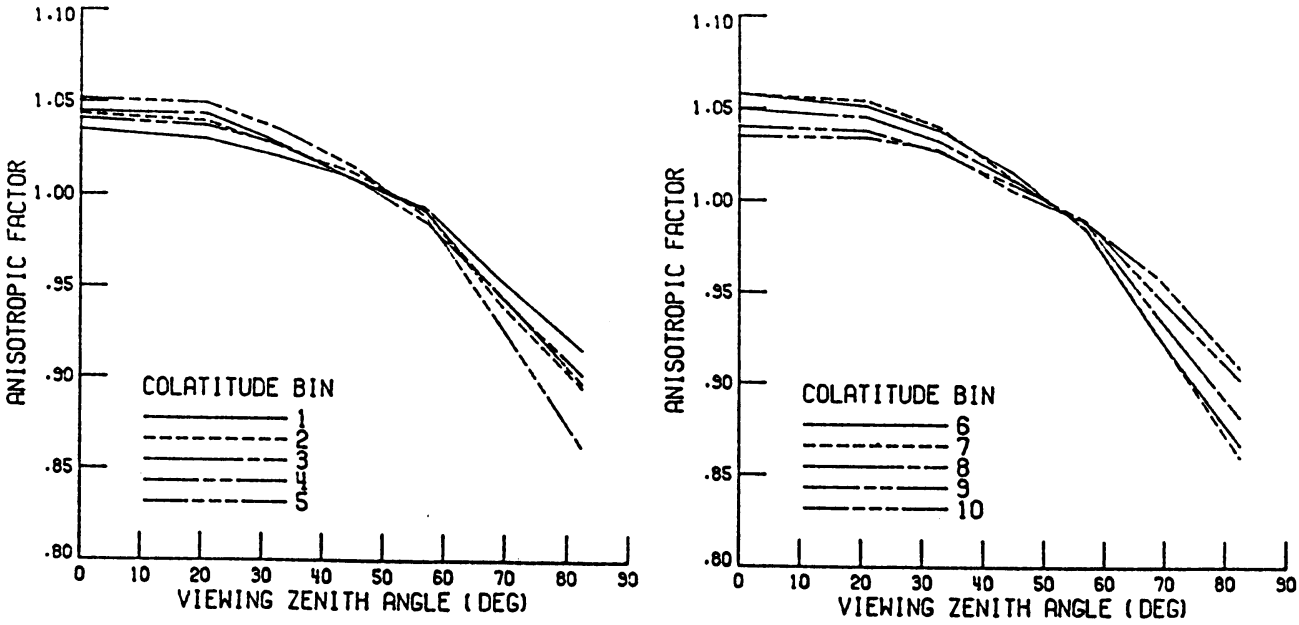

Fig. 11b. As in Fig. 11a), partly cloudy.

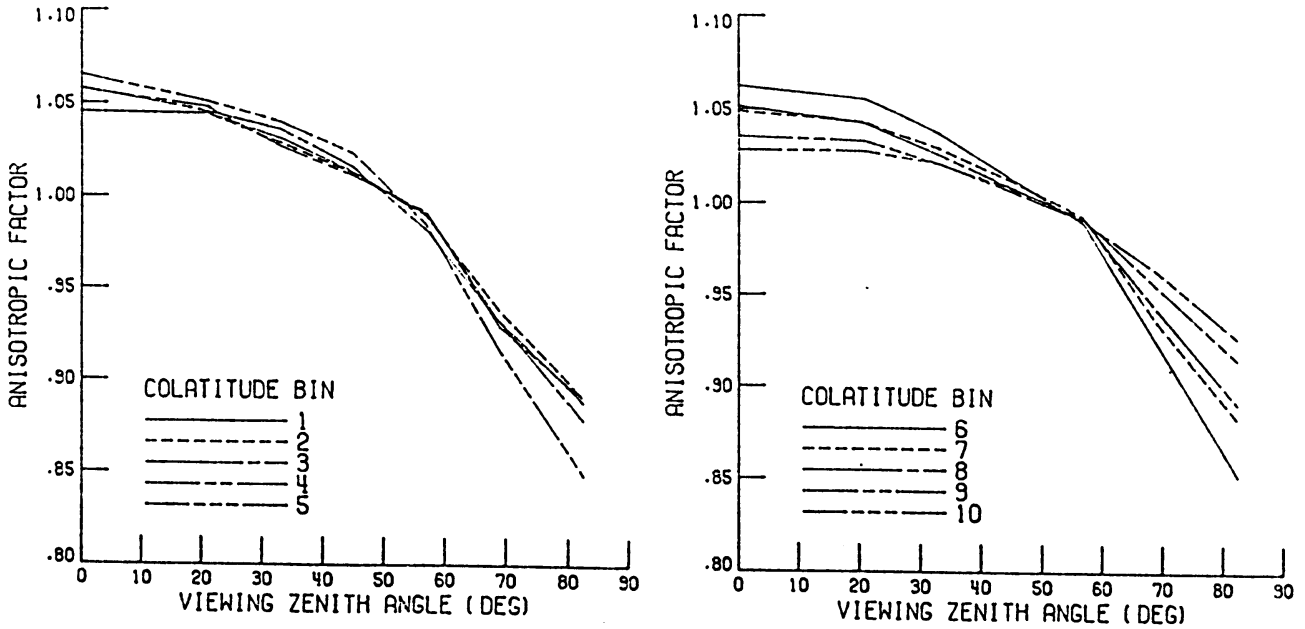

Fig. 11c. As in Fig. 11a), mostly cloudy.

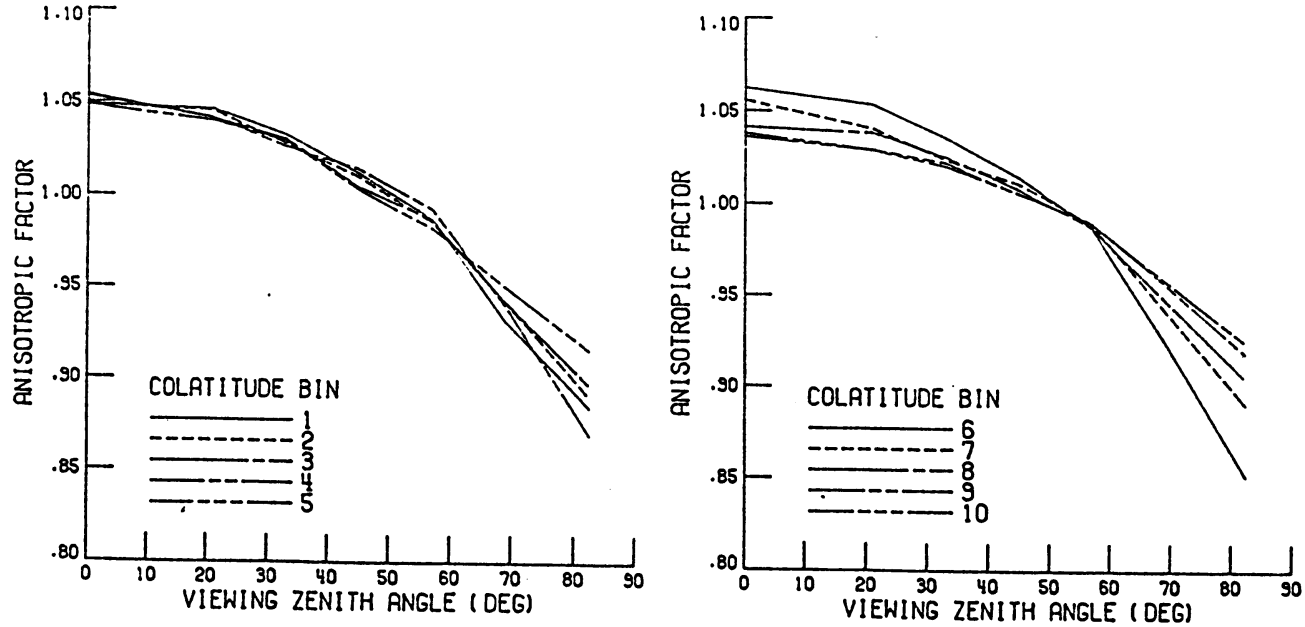

Fig. 11d. As in Fig. 11a), overcast.

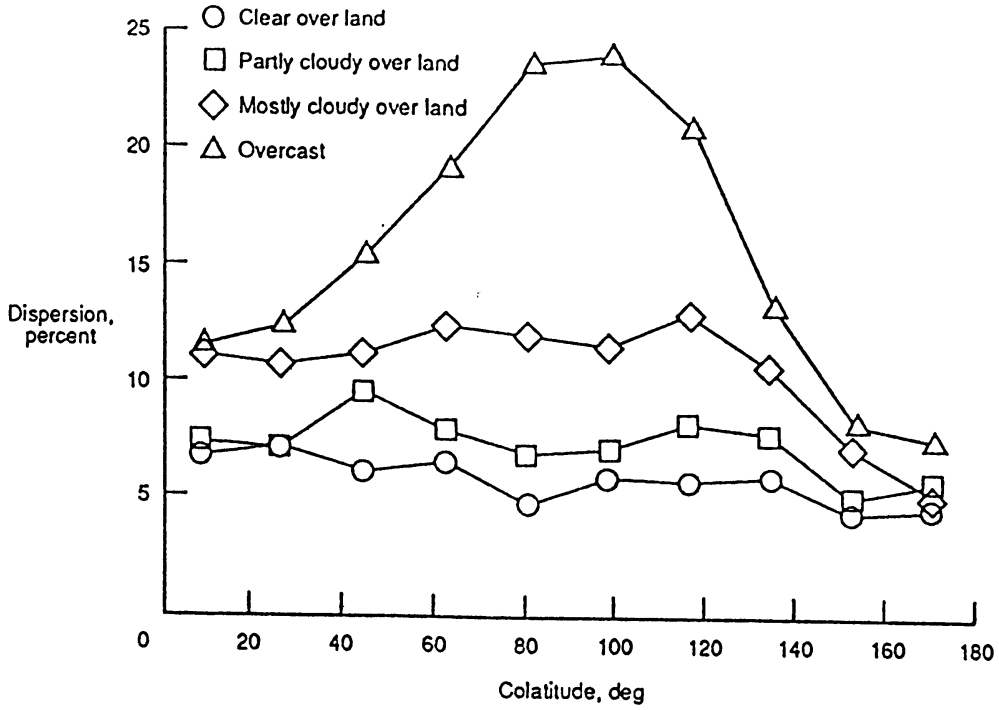

Fig. 12a. Dispersion of longwave radiance in winter averaged over day, night and viewing zenith angles over land.

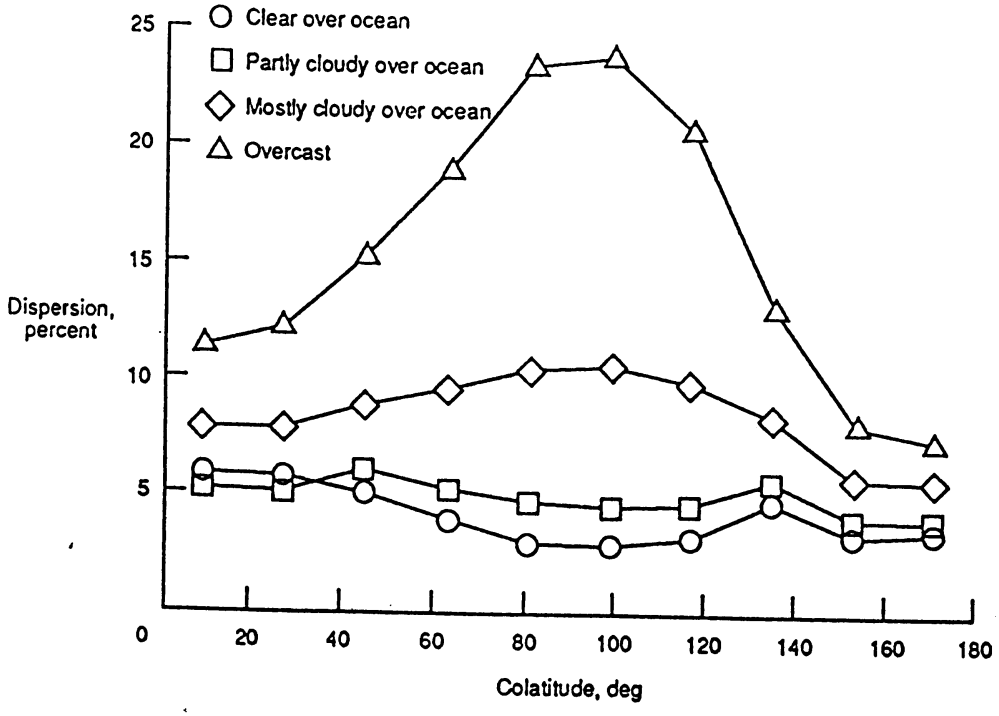

Fig. 12b. As in Fig. 12a), over ocean.

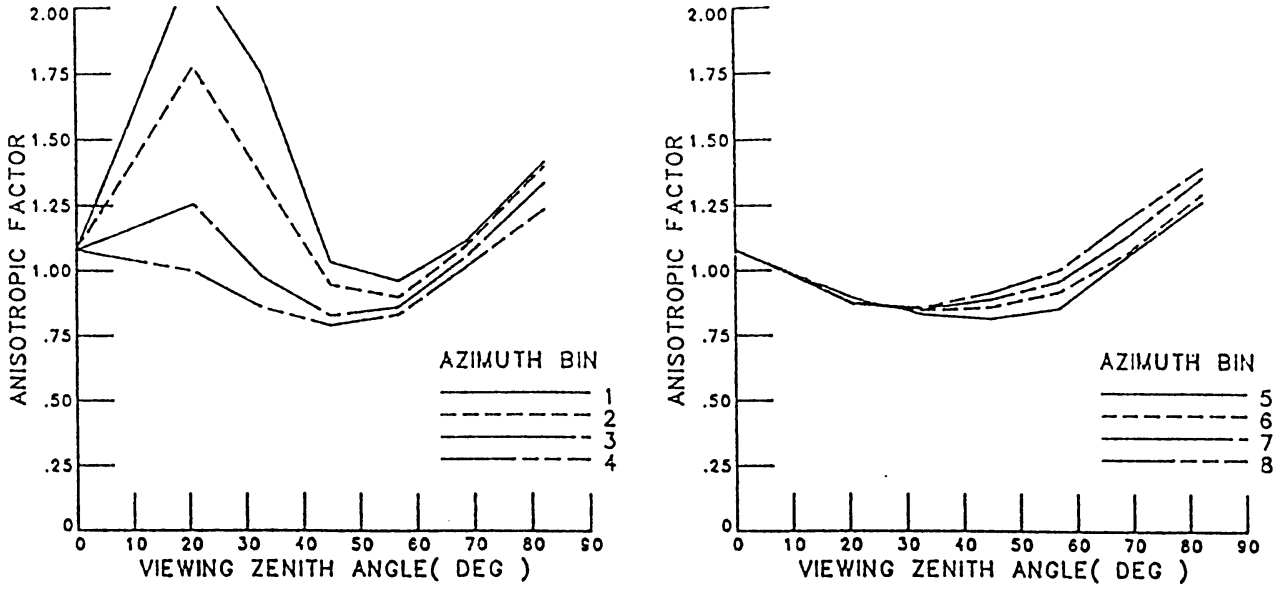

Fig. 13a. Anisotropic factor, R, for clear sky over ocean; Solar zenith angle is between 0 and 26 deg. Azimuth bins indicate azimuth angle ranges: bin 1 is related to forward reflected SW radiation, bin 8 is related to backward reflection. Azimuth is as defined in fig. 2.

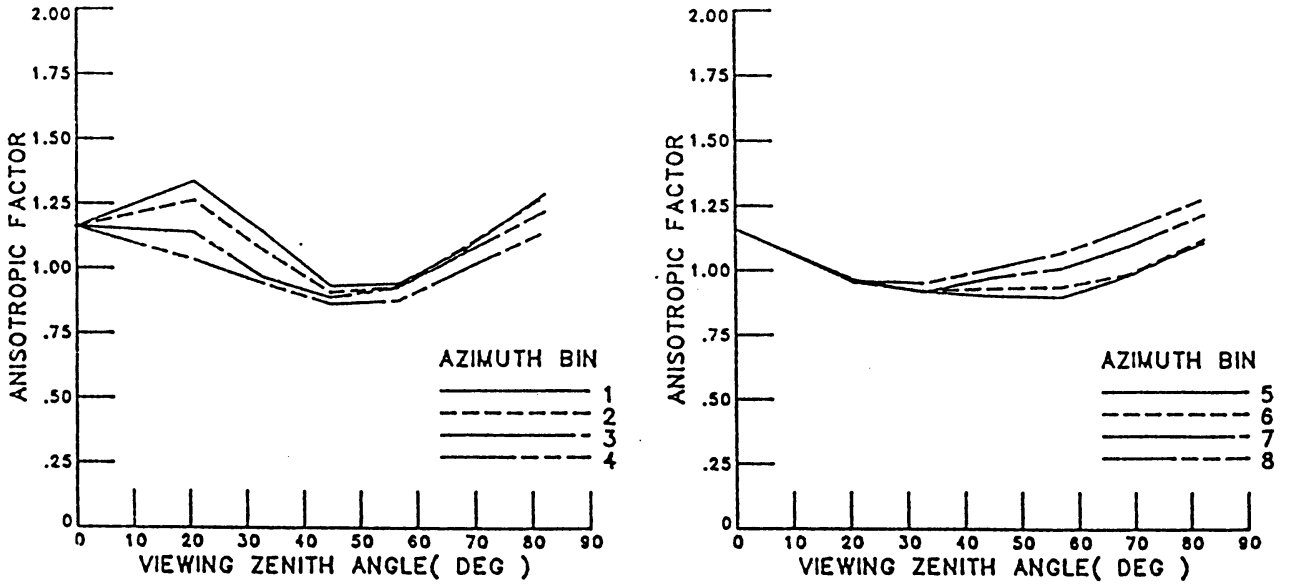

Fig. 13b. As in Fig. 13a), partly cloudy over ocean

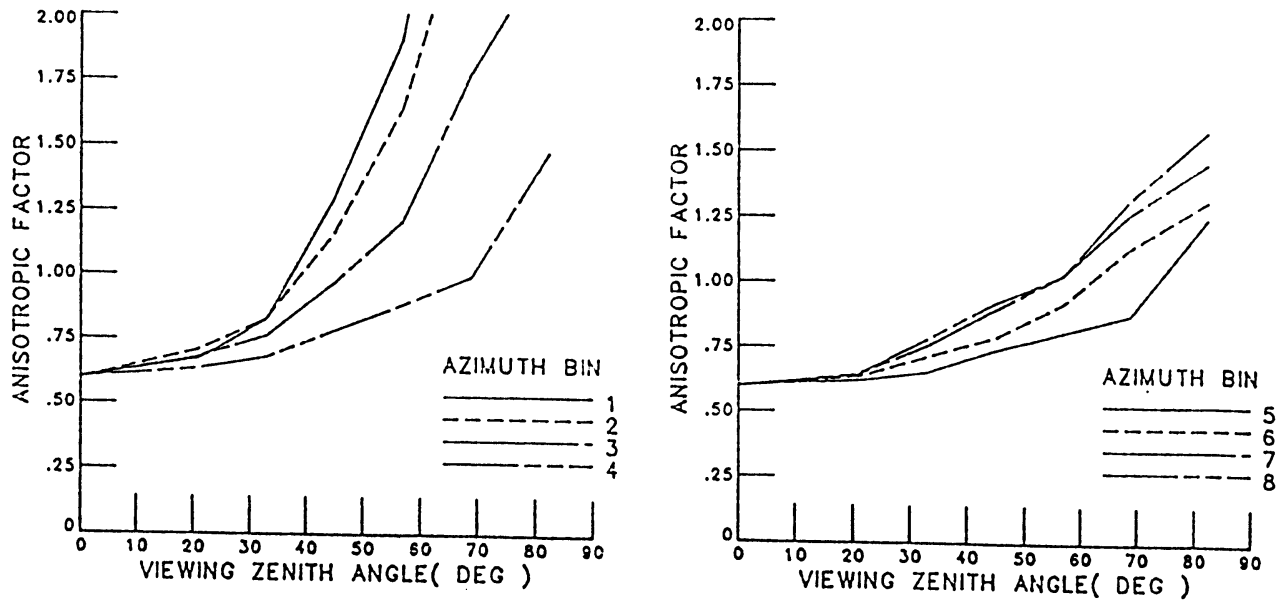

Fig. 13c. As in Fig. 13a), mostly cloudy over ocean and solar zenith angle between 73 and 78 deg.

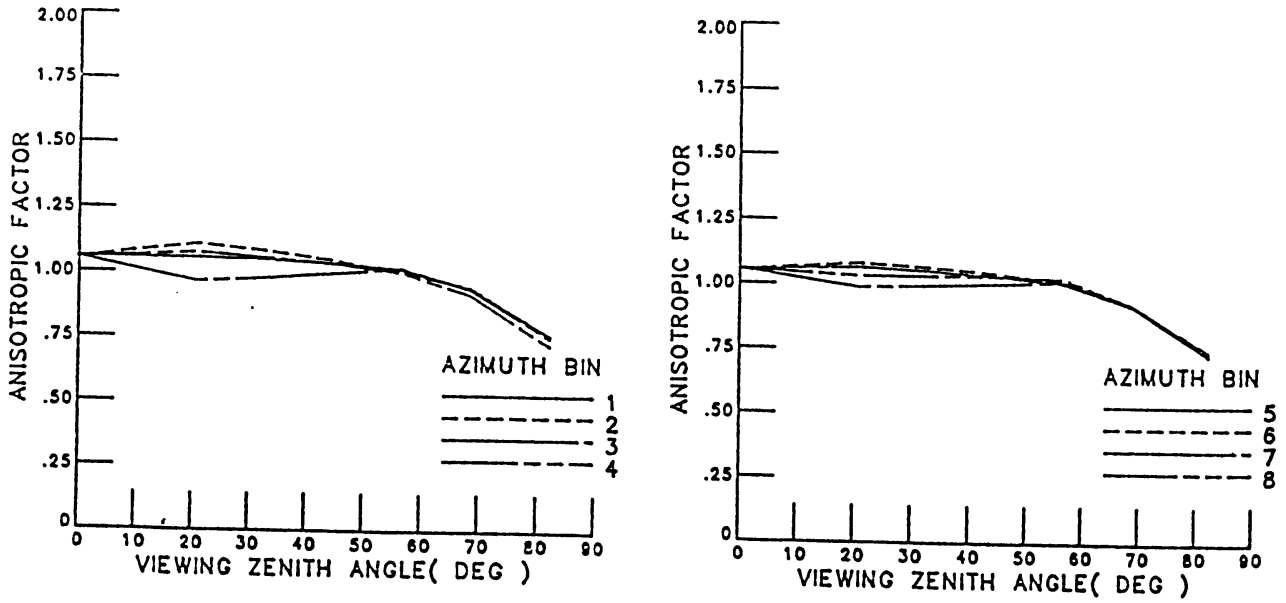

Fig. 13d. As in Fig. 13a), clear over snow, solar zenith angle between 0 and 26 deg.

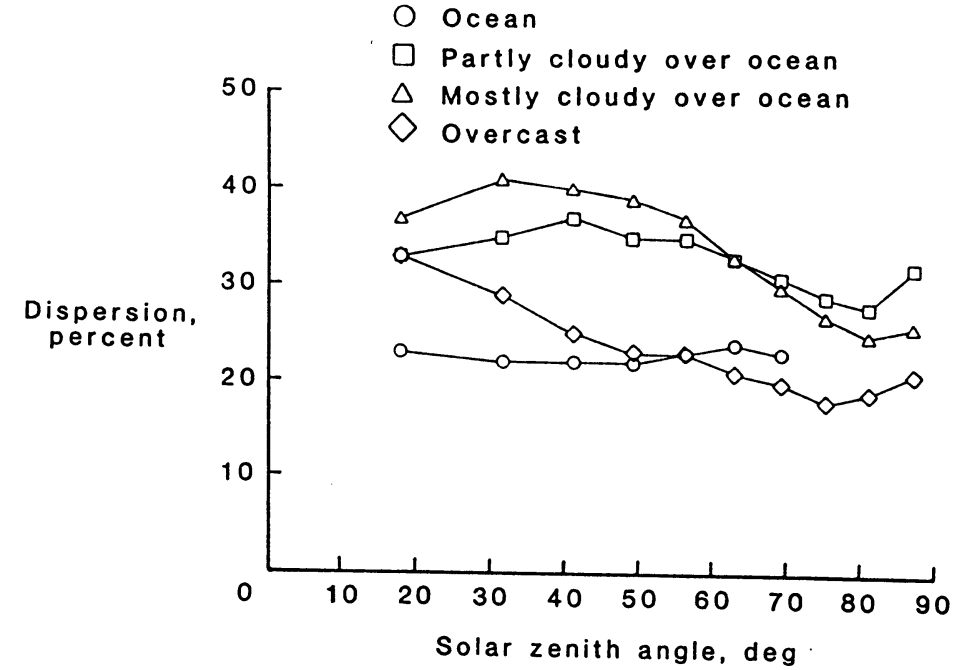

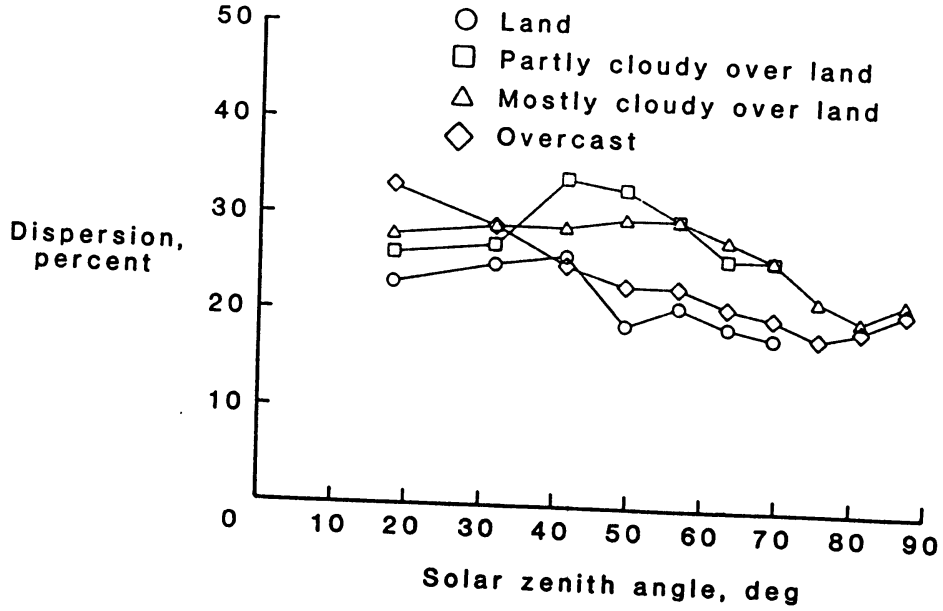

Fig. 14. Dispersion of the shortwave anisotropic factor averaged over all viewing angles and azimuths.

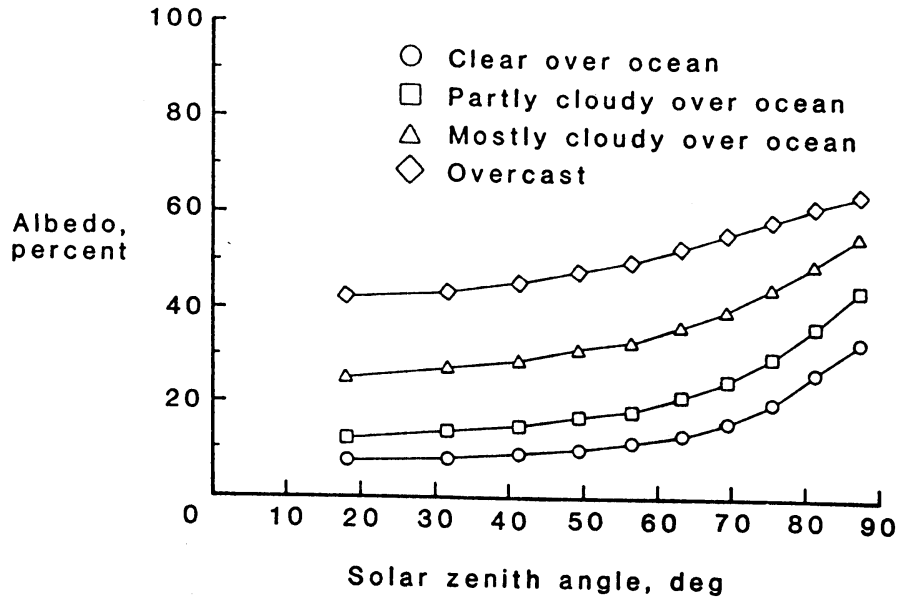

Fig. 15a. Albedo over ocean.

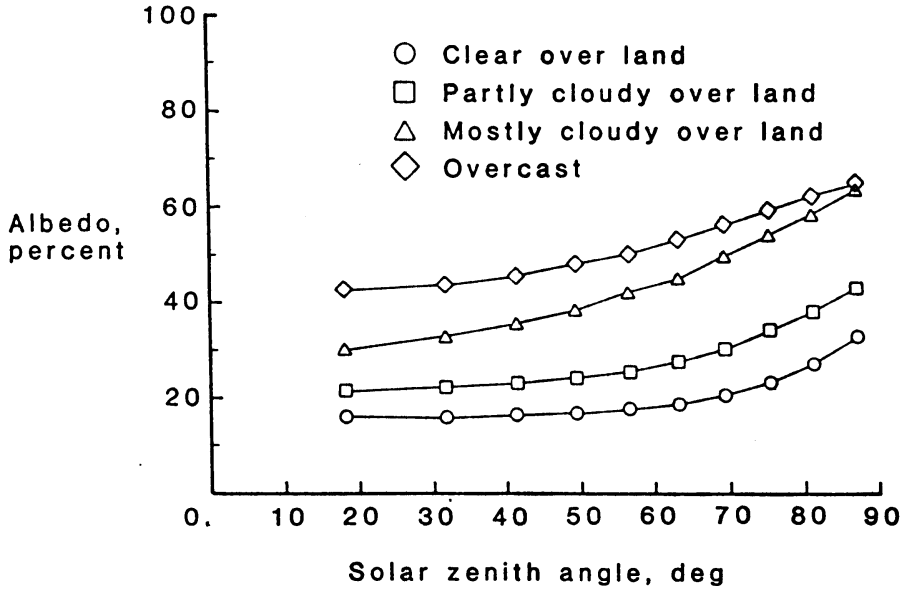

Fig. 15b. Albedo over land.

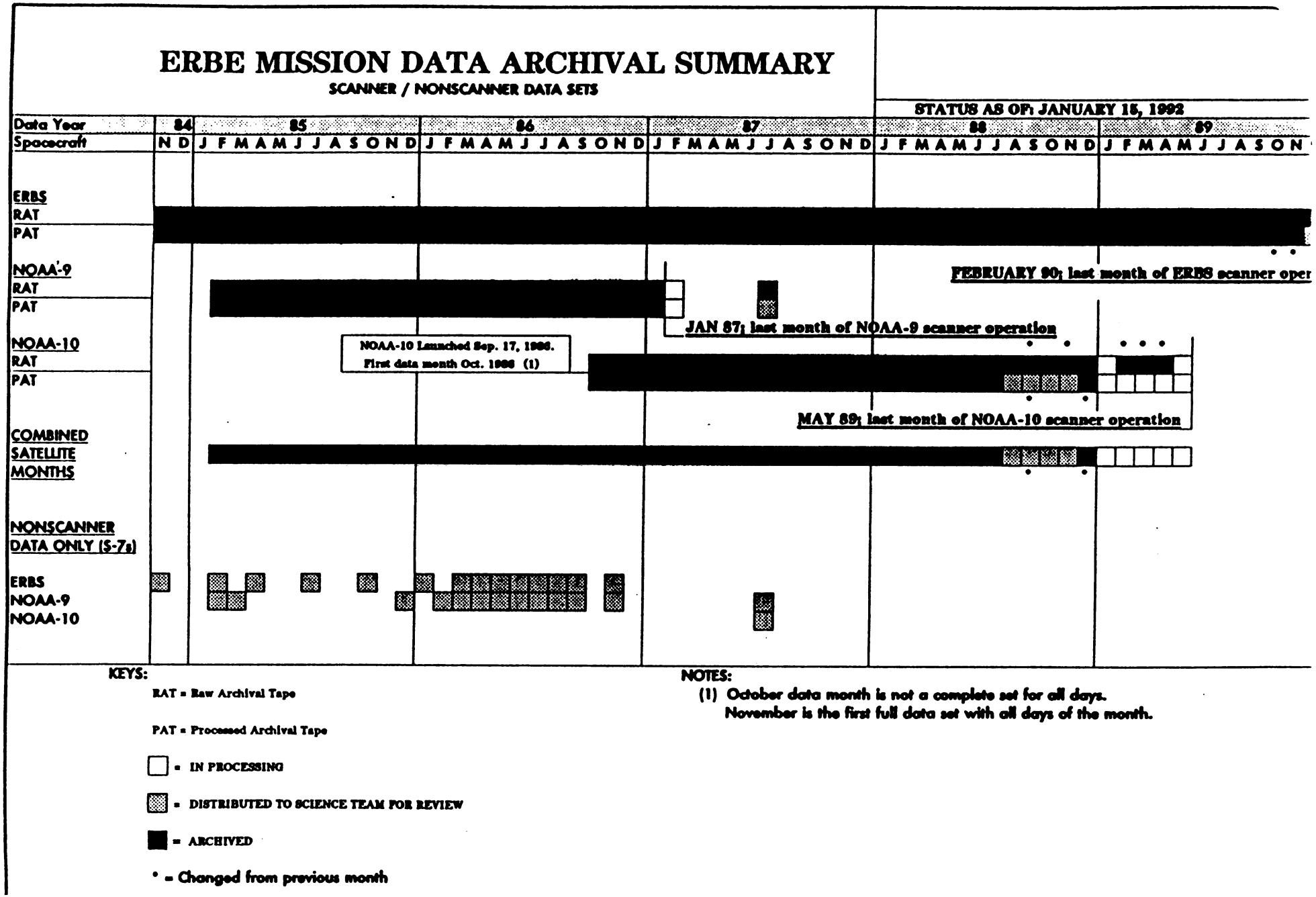

Fig. 16. Status of the ERBE data archival as of January 1992.